Numerical methods for plasma sheaths

Valentin Ayot[*], Averil Prost[†], Christian Tayou-Fotso[‡]

Abstract

This article is a report of the project achieved during the CEMRACS 2022. We consider Vlasov-Poisson model for a two-species plasma. Our aim is to extend an existing code from periodic boundary conditions to nonperiodic boundary conditions. In particular, we focus on the interaction of the plasma with a non-emitting wall, and wish to capture the physical phenomenon called *Debye sheath*. Comparison between this numerical scheme and a finite difference scheme are presented.

1 Plasma sheaths

Plasmas are neutral at the equilibrium in a sufficiently large domain. However, near a boundary, a charge imbalance may be observed in a thin layer called *sheath*. This phenomenon stems from the interaction of ions and electron with the boundary media (a cold metallic wall, for instance). Both species will be absorbed by the wall, but with a rate proportional to their speed. Since the electrons are moving several order of magnitude faster than the ions, a positively charged layer (the *Debye sheath*) forms near the boundary.

The difference of speed between both species is numerically challenging, since a wide range of velocities is needed to correctly model the evolution of electrons, but accuracy is required on low velocities to capture the ions. When using mesh-based approaches, it is tempting to use adapted velocity meshes for the different species. This requires the choice of an interpolation procedure: several possibilities are found in the literature, as uniform cubic splines in the GYSELA code [GAB+16] and extension to non-uniform splines in [BMG+], or high-order polynomial interpolation [BBC21]. We will follow the latter method.

Our purpose is to investigate numerically the formation of the sheath. It follows previous work of Michel Mehrenberger and Yann Barsamian **is there a reference for the existing code?** on a periodic case, and of [BMN] on a collisional model. Our aim is to study an ionization model with nonperiodic boundary conditions, thus extending the work of **Michel and Yann - how to say it properly?**. The first section introduces the corresponding system, and derives the boundary conditions. The second section presents the numerical methods used to simulate the evolution of the plasma, and the third section gives some results and comparisons.

The model Let $t \in \mathbb{R}^+$ denote the time variable, $x \in [-1, 1]$ denote the spatial variable in a normalized one-dimensional domain, and $v \in \mathbb{R}$ denote the speed variable. The distribution of species is described through their density in the phase space, denoted by $f_i : (t, x, v) \in \mathbb{R}^+ \times [-1, 1] \times \mathbb{R} \mapsto \mathbb{R}$ for the ions, and $f_e : (t, x, v) \in \mathbb{R}^+ \times [-1, 1] \times \mathbb{R} \mapsto \mathbb{R}$ for the electrons. To these kinetic quantities, we add the spatial densities $n_{i,e}$ and currents $J_{i,e}$, defined by

$$n_{i,e}(t, x) \coloneqq \int_{v\in\mathbb{R}} f_{i,e}(t, x, v)dv, \quad \text{and} \quad J_{i,e}(t, x) \coloneqq \int_{v\in\mathbb{R}} v f_{i,e}(t, x, v)dv. \tag{1.1}$$

[*]Institut de Mathématiques, CNRS, UMR 5251, Université de Bordeaux, F-33405 Talence, France. valentin.ayot@u-bordeaux.fr

[†]INSA de Rouen, LMI (EA 3226 - FR CNRS 3335), 685 Avenue de l'Université, 76801 St Etienne du Rouvray cedex, France. averil.prost@insa-rouen.fr

[‡]Labo. J. A. Dieudonné, UMR 6621, Université Nice-Sophia Antipolis, Parc Valrose, F-06108 Nice cedex 02, France. christian.tayou-fotso@unice.fr

In the sequel, we will denote $n(t,x) \coloneqq n_i(t,x) - n_e(t,x)$, and $J(t,x) \coloneqq J_i(t,x) - J_e(t,x)$.

The evolution of the densities is modelled by the Vlasov-Poisson equations. Let $\varphi : \mathbb{R}^+ \times [-1,1] \mapsto \mathbb{R}$ denote the electric potential. Then

$$\begin{cases} \partial_t f_i + v\partial_x f_i - \partial_x\varphi\,\partial_v f_i = \nu f_e & (t,x,v) \in \mathbb{R}_*^+ \times]-1,1[\times\mathbb{R}, \quad (1.2a) \\ \partial_t f_i + v\partial_x f_e + \dfrac{\partial_x\varphi}{\mu}\,\partial_v f_e = 0 & (t,x,v) \in \mathbb{R}_*^+ \times]-1,1[\times\mathbb{R}, \quad (1.2b) \\ -\lambda^2\partial_{xx}^2\varphi = n(t,x) & (t,x) \in \mathbb{R}^+ \times]-1,1[. \quad (1.2c) \end{cases}$$

The physical parameters ν, μ and λ have the following meaning:

- $\nu \geqslant 0$ is the ionization frequency. It describes the rate of **creation / production / injection ?** of ions in presence of electrons.
- $\mu \coloneqq m_e/m_i$ is the mass ratio between electrons and ions.
- $\lambda > 0$ is the Debye length.

In the sequel, we may use the electric field $E(t,x) \coloneqq -\partial_x\varphi(t,x)$ in place of the potential. The, the second-order Poisson equation rewrites as

$$\lambda^2\partial_x E(t,x) = n(t,x) \qquad (t,x) \in \mathbb{R}^+ \times]-1,1[. \tag{1.3}$$

Remark 1.1. *To reduce the notations, we will use f_s, $s \in \{i,e\}$ to denote both the electronic and ionic distributions. The advection equations* (1.2a) *and* (1.2b) *rewrite*

$$\partial f_s + v\partial_x f_s - c_s\partial_x\varphi\partial_v f_s = S_s,$$

with the speed coefficients c_s and source terms S_s defined as

$$c_i \coloneqq 1, \quad c_e \coloneqq -\frac{1}{\mu}, \quad S_i \coloneqq \nu f_e, \quad S_e \coloneqq 0.$$

The densities f_i and f_e are subject to initial and boundary conditions, given by

$$\begin{cases} f_s(0,x,v) \coloneqq f_s^0(x,v) & (x,v) \in]-1,1[\times\mathbb{R}, \quad (1.4a) \\ f_s(t, x = \pm 1, \pm v < 0) \coloneqq 0 & t \in \mathbb{R}_*^+. \quad (1.4b) \end{cases}$$

The homogeneous boundary condition (1.4b) stems from the non-emitting wall model: the boundary absorbs particles without any reflection.

To completely describe the model, we still need to provide boundary conditions for the Poisson problem (1.2c). A first one is given by the choice of a reference potential

$$\varphi(t,0) = 0 \qquad \forall t \in \mathbb{R}^+. \tag{1.5}$$

To derive a second boundary condition, we introduce a fundamental symmetry assumption.

Symmetry We will look for *symmetric solutions* satisfying

$$\varphi(t,x) = \varphi(t,-x) \qquad (t,x) \in \mathbb{R}^+ \times [-1,1]. \tag{1.6}$$

By derivation with respect to $x \in]-1,1[$, we immediately obtain

$$\partial_x\varphi(t,x) = -\partial_x\varphi(t,-x), \quad \text{i.e.} \quad E(t,x) = -E(t,-x).$$

In particular, the electric field vanishes at $x = 0$, and the Neumann boundary condition

$$\partial_x \varphi(t, 0) = 0 \quad \text{or equivalently} \quad E(t, 0) = 0 \tag{1.7}$$

may be used (with (1.5)) to close the Poisson equation (1.2c).

Let us notice that the advection equations (1.2a) and (1.2b) are driven by the vector fields

$$(t, x, v) \to (1, v, E(t, x)) =: V_i(t, x, v) \quad \text{and} \quad (t, x, v) \to (1, v, -E(t, x)/\mu) =: V_e(t, x, v).$$

Both these fields satisfy the radial symmetry $V_s(t, x, v) = V_s(t, -x, -v)$. In consequence, if we assume that $f_s^0(x, v) = f_s^0(-x, -v)$, the solutions $f_s(t, x, v)$ will be radially symmetric around $(t, 0, 0)$, i.e.

$$f_i(t, x, v) = f_i(t, -x, -v) \quad \text{and} \quad f_e(t, x, v) = f_e(t, -x, -v) \quad \forall (t, x, v) \in \mathbb{R}^+ \times [-1, 1] \times \mathbb{R}.$$

In particular, we have

$$n_s(t, x) = \int_{v\in\mathbb{R}} f_s(t, x, v)dv = \int_{w\in\mathbb{R}} f_s(t, x, -w)dw = \int_{w\in\mathbb{R}} f_s(t, -x, w)dw = n_s(t, -x), \quad \text{and}$$
$$J_s(t, x) = \int_{v\in\mathbb{R}} v f_s(t, x, v)dv = -\int_{w\in\mathbb{R}} w f_s(t, x, -w)dw = -\int_{w\in\mathbb{R}} w f_s(t, -x, w)dw = -J_s(t, -x).$$

Remark 1.2 (Additional symmetry of f_e)**.** *Notice that the function $f : (t, x, v) \to f_e(t, x, v) - f_e(t, x, -v)$ satisfies the linear equation*

$$0 = \partial_t f(t, x, v) + v\partial_x f(t, x, v) - \frac{E(t, x)}{\mu}\partial_v f(t, x, v).$$

The boundary condition (1.4b) *gives $f(t, \pm 1, \pm v < 0) = 0$. If, in addition, we assume that the initial condition f_e^0 satisfies $f_e^0(x, v) - f_e^0(x, -v) = 0$, then we obtain*

$$f_e(t, x, v) = f_e(t, x, -v) \quad \forall (t, x, v) \in \mathbb{R}^+ \times [-1, 1] \times \mathbb{R}. \tag{1.8}$$

Deriving a boundary condition at $x = \pm 1$ The centered Neumann condition (1.7) enforces continuity of$\partial_x \varphi$ at $x = 0$. We may avoid this constraint by deriving another Neuman condition, given on the boundary $x = \pm 1$.

First, we derive with respect to time the Poisson equation (1.2c)

$$-\partial_t(\lambda^2 \partial_{xx}^2 \varphi) = \partial_t n,$$

and considering the difference between the v-integration of the Vlasov equations (1.2a) and (1.2b) gives

$$\partial_t n = \nu n_e - \partial_x J,$$

so that, using $E = -\partial_x \varphi$, we get

$$\partial_x(\lambda^2 \partial_t E + J) = \nu n_e, \quad \forall x \in]-1, 1[.$$

Integrating now in space leads to

$$\lambda^2 \partial_t E(t, 1) + J(t, 1) = \lambda^2 \partial_t E(t, -1) + J(t, -1) + \nu \int_{-1}^{1} n_e(t, x)dx, \tag{1.9}$$

and using the symmetries $E(t, 1) = -E(t, -1)$ and $J(t, 1) = -J(t, -1)$, it comes

$$\lambda^2 \partial_t E(t, \pm 1) + J(t, \pm 1) = \pm\frac{\nu}{2} \int_{-1}^{1} n_e(t, x)dx. \tag{1.10}$$

Time integration gives a condition of the form $\partial_x \varphi(t, \pm 1) = C_\pm(t)$, where

$$C_\pm(t) \coloneqq \partial_x \varphi(0, \pm 1) + \frac{1}{\lambda^2} \int_0^t J(s, \pm 1)ds \mp \frac{\nu}{2\lambda^2} \int_0^t \int_{-1}^{1} n_e(s, x)dxds. \tag{1.11}$$

2 Numerical methods

2.1 Poisson equation

The Poisson problem is solved with integral representations of the variable E.

First, we consider the centered Neumann boundary condition (1.7). Then, integrating the Poisson problem (1.3) over $[0, x]$ yields

$$E(t,x) = 0 + \int_0^x n(t,y)dy = \int_0^x \int_{v\in\mathbb{R}} [f_i(t,y,v) - f_e(t,y,v)]dvdy. \tag{2.1}$$

Let us now consider the boundary condition (1.10). The spacial domain $[-1, 1]$ is split into its positive and negative part, and integrating (1.3) gives

$$E(t,x) = \begin{cases} E(t,\ \ 1) - \int_x^1\ n(t,y)dy = -C_+(t) - \int_x^1\ \int_{v\in\mathbb{R}}[f_i(t,y,v) - f_e(t,y,v)]dvdy & x \in [0,1] \\ E(t,-1) + \int_{-1}^x n(t,y)dy = \ \ C_-(t) + \int_{-1}^x \int_{v\in\mathbb{R}}[f_i(t,y,v) - f_e(t,y,v)]dvdy & x \in [-1,0[\end{cases} \tag{2.2}$$

Note that here, the electric field may "jump" at $x = 0$. Both expressions may be approximated by quadrature formulas.

2.2 Finite Differences (FD)

Define a numerical computation domain $\Omega \coloneqq [-1, 1] \times [-\overline{V}, \overline{V}]$, with a large enough maximum speed $\overline{V}$. Let $(x_j, v_k)_{k\in[\![0,K]\!]}^{j\in[\![0,J]\!]}$ be a cartesian grid of Ω of step $(\Delta x, \Delta v)$. We discretize the advection equations on the subgrid $(x_j, v_k)_{k\in[\![1,K-1]\!]}^{j\in[\![1,J-1]\!]}$ by an explicit Euler scheme in time, and the upwind scheme in space:

$$\frac{f_{s,j,k}^{n+1} - f_{s,j,k}^n}{\Delta t} + D_{j,k}^- f_s^n \begin{pmatrix} v_k \\ c_s E_j^n \end{pmatrix}_+ + D_{j,k}^+ f_s^n \begin{pmatrix} v_k \\ c_s E_j^n \end{pmatrix}_- = S_{s,j,k}^n, \tag{2.3}$$

where $a_+ = \max(a, 0)$ and $a_- = \min(a, 0)$ are respectively the pointwise positive and negative parts, and the decentered discrete differences are defined as

$$D_{j,k}^{\pm} f \coloneqq \pm\left(\frac{f_{j\pm1,k} - f_{j,k}}{\Delta x}, \frac{f_{j,k\pm1} - f_{j,k}}{\Delta v}\right).$$

The values of $f_{s,j,k}^n$ on the boundary are taken as follows:

- the boundary condition (1.4b) yields $f_{s,j,k}^n = 0$ whenever $x_j = -1, v_k > 0$ or $x_j = 1, v_k < 0$.
- It is considered that $\overline{V}$ is large enough to take the values on the speed boundary $v_k = \pm\overline{V}$ equal to 0.
- The remaining values $f_{s,j,k}^n$, $x_j = -1, -\overline{V} < v_k \leqslant 0$ or $x_j = 1, 0 \leqslant v_k < \overline{V}$ may be computed using the scheme (2.3), since the sign of the speed allows to use only inner points.

The upwind scheme is known to be diffusive, and stable under the CFL condition

$$1 - \max_k |v_k| \frac{\Delta t}{\Delta x} - |c_s| \max_j |E_j^n| \frac{\Delta t}{\Delta v} \geqslant 0 \quad \forall s \in \{i, e\} \text{ and } n \in [\![1, N]\!].$$

Given Δx and Δv, we deduce a sufficiently small value of Δt with the bound

$$\Delta t \leqslant \min\left(\frac{\Delta x}{\overline{V}}, \min(1,\mu)\frac{\Delta v}{E_{\max}}\right), \quad E_{\max} > 0 \text{ postulated } \textit{a priori}.$$

2.3 Semi-Lagrangian (SL)

The full model (1.2) nicely lends itself to approximation by time splitting. Indeed, consider the following Strang splitting decomposition.

$$\begin{array}{ll}
\dfrac{\Delta t}{2} & \begin{cases} \partial_t f_s + v\partial_x f_s = 0 & \text{Linear advection along } x, \\ \lambda^2 \partial_x E = n_i - n_e & \text{Poisson problem,} \end{cases} \\
\dfrac{\Delta t}{2} & \partial_t f_i = \nu f_e \qquad \text{Ionization,} \\
\Delta t & \partial_t f_s + c_s E \partial_v f_s = 0 \quad \text{Linear advection along } v, \\
\dfrac{\Delta t}{2} & \partial_t f_i = \nu f_e \qquad \text{Ionization,} \\
\dfrac{\Delta t}{2} & \begin{cases} \lambda^2 \partial_x E = n_i - n_e & \text{Poisson problem,} \\ \partial_t f_s + v\partial_x f_s = 0 & \text{Linear advection along } x. \end{cases}
\end{array}$$

Each of the splitting step may be solved exactly. Indeed, the Poisson problems are solved by the integral representations (2.1) and (2.2). The ionization steps are pointwise ODE with time-independant source term, and are exactly solved by the explicit Euler scheme. Finally, notice that each advection is at constant speed with respect to the advection variable. This allows for the use of elementary 1D solvers.

Numerical treatment of the boundaries Let us focus on the elementary advection equation with constant speed $a > 0$

$$\partial_t f(t,x) + a\partial_x f(t,x) = 0, \quad f(t,-1) = 0, \quad \forall (t,x) \in \mathbb{R}_*^+ \times]-1,1[.$$

Let $(x_j)_{j\in[\![0,J]\!]}$ be a space mesh of step $\Delta x \coloneqq 2/J$, and $(t_n)_{n\in[\![0,N]\!]}$ be a time mesh of step $\Delta t \coloneqq T/N$. We follow the work of [CL20], and consider a semi-Lagrangian scheme defined as

$$f_j^{n+1} = \text{Lagrange interpolation}\,(f^n, x_j - a\Delta t) \coloneqq \sum_{k=-d}^{d} f_{j+k}^n L_k(x_j - a\Delta t),$$

with $(L_k)_{k\in[\![-d,d]\!]}$ the Lagrange polynomes satisfying $L_k(x_l) = \delta_{kl}$. The stencil of the Lagrange interpolation uses $2d+2$ points, where $d \in \mathbb{N}$. The boundaries are treated as follow:

- the *inflow* side, corresponding to $x = -1$, relies on the analytical solution $f(t,x) = 0\ \forall x \leqslant at$. Whenever the scheme needs a value f_j^n with $j < 0$, it may be exactly taken equal to 0.
- in the case $d > 0$, the Lagrange stencil may also need *outflow* values f_j^n with $j > J$. Such values may be determined by polynomial extrapolation. Let $k_b \in \mathbb{N}$, and let p be the unique polynomial of order k_b interpolating (x_j, f_j^n) for $j \in [\![J-kb, J]\!]$. The *outflow ghost points* will be defined by $f_j^n \coloneqq p(-1+j\Delta x)$ $\forall j > N$.

3 Numerical results

3.1 1-species validation test case

We rely on the work of [MK20] to provide an analytical solution in a 1-species case. Consider the simplified stationary model describing the density of particles $f = f(t,x,v)$, and the potential $\varphi = \varphi(t,x)$:

$$\begin{cases} \partial_t f + v\partial_x f - \partial_x\varphi\partial_v f = 0 & (t,x,v) \in \mathbb{R}_*^+ \times]-1,1[\times\mathbb{R}, \qquad (3.1a) \\ \partial_{xx}^2 \varphi = \displaystyle\int_{v\in\mathbb{R}} f dv & (t,x) \in \mathbb{R}^+ \times]-1,1[. \qquad (3.1b) \end{cases}$$

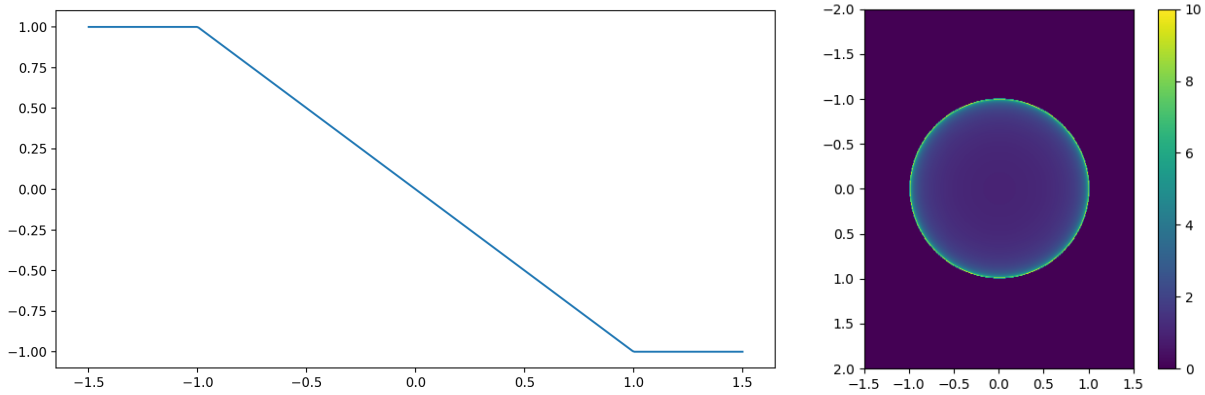

Figure 1: Malkov solutions (3.4) on $[-1.5, 1.5]$. Right: electric field E. Left: density f.

The electric field is extended outside of $[-1, 1]$ by a constant. The density f is represented in the domain $[-1.5, 1.5] \times [-2, 2]$, and truncated to 10.

The initial and boundary conditions are given by

$$\begin{cases} f(0, x, v) \coloneqq f^0(x, v), \quad f(t, x = \pm 1, \pm v < 0) = 0 & \text{(3.2a)} \\ \varphi(t, 0) = \partial_x \varphi(t, 0) = 0 & \text{(3.2b)} \end{cases}$$

This model may be seen as a particular case of the two-species Vlasov-Poisson (1.2), upon taking the following parameters:

$$f_i^0 \equiv 0, \quad \nu = 0, \quad \mu = -1, \quad \lambda = 1, \quad f_e^0 = f^0.$$

The reader may verify that (3.1) is solved in $\mathbb{R}^+ \times [-1, 1] \times \mathbb{R}$ by the following stationary couple:

$$f(t, x, v) \coloneqq \begin{cases} \frac{1}{\pi} \left(1 - x^2 - v^2\right)^{-1/2} & \text{if } x^2 + z^2 < 1 \\ 0 & \text{otherwise} \end{cases}, \quad \text{and} \quad \varphi(t, x) \coloneqq \frac{x^2}{2}. \tag{3.3}$$

It is numerically relevant to extend the Malkov solution (3.3) to spatial domains $x \in [-1 - \varepsilon, 1 + \varepsilon]$ by

$$f(t, x, v) \coloneqq \begin{cases} \frac{1}{\pi} \left(1 - x^2 - v^2\right)^{-1/2} & \text{if } x^2 + z^2 < 1 \\ 0 & \text{otherwise} \end{cases}, \quad \text{and} \quad \varphi(t, x) \coloneqq \min\left(\frac{x^2}{2}, \frac{|x|}{2}\right). \tag{3.4}$$

Figure (1) illustrates the stationary solutions.

For now, I don't reach order 1. Maybe bug?

Parameters			Errors	
N_x	N_v	N_t	L^∞	L^1
100	2049	1281	8.59e-03	6.22e-03
200	2049	1281	1.22e-02	1.78e-02
400	2049	1281	6.22e-03	9.07e-03
800	2049	1281	7.13e-03	7.23e-03
100	4097	2561	5.65e-03	4.92e-03
200	4097	2561	3.88e-03	4.70e-03
400	4097	2561	4.08e-03	5.77e-03
800	4097	2561	2.39e-03	2.93e-03

Table 1: DF errors for Malkov test case.

Parameters			Errors	
N_x	N_v	N_t	L^∞	L^1
100	201	1000	1.30e-02	1.59e-03
200	401	1000	1.66e-02	1.88e-03
400	801	1000	1.88e-02	1.35e-03
800	1601	1000	6.15e-03	2.66e-04
100	101	100	3.19e-02	3.45e-03
200	201	200	2.77e-02	3.13e-03
400	401	400	6.49e-03	4.35e-04
800	801	800	1.51e-02	8.50e-04
1600	1601	1600	6.57e-03	2.50e-04
100	2049	10000	4.06e-03	4.62e-04
200	2049	10000	1.72e-02	1.40e-03
400	2049	10000	7.88e-03	3.90e-04
800	2049	10000	1.12e-02	5.37e-04
1000	201	5000	1.00e-02	3.32e-04
1000	401	5000	1.16e-02	5.48e-04
1000	801	5000	5.01e-03	1.72e-04
1000	1601	5000	6.34e-03	3.25e-04

Table 2: SL errors for Malkov test case.

3.2 Comparison between (SL) and (FD)

In the sequel, we use the following physical parameters:

$$\lambda = \frac{1}{2}, \quad \mu = \frac{1}{100}, \quad \text{and} \quad \nu = 20. \tag{3.5}$$

The initial conditions are chosen as the thermodynamic equilibrium in an infinite spatial domain, or in a domain with periodic condition. The densities are then given by

$$f_i^0(x,v) \coloneqq \frac{\exp\left(-\frac{v^2}{2}\right)}{\sqrt{2\pi}}, \quad \text{and} \quad f_e^0(x,v) \coloneqq \sqrt{\mu}\frac{\exp\left(-\mu\frac{v^2}{2}\right)}{\sqrt{2\pi}}.$$

In order to satisfy the boundary conditions, we multiply $f_{i,e}$ by a mask, defined as

$$\text{mask}(x,v) \coloneqq \frac{1}{2}\left(\tanh\left(\frac{x-(-0.8)}{0.1}\right) - \tanh\left(\frac{x-0.8}{0.1}\right)\right).$$

Figure (2) illustrates the resulting initial conditions.

Short time The simulations run over the spatial domain $x \in [-1,1]$. The semi-Lagrangian code computes the electron velocities on $v_e \in [-50,50]$, and ion velocities on $v_i \in [-8,8]$. The finite differences code uses the same mesh for ions and electrons, chosen as $v \in [-50,50]$. To simplify the comparison, visualisations of f_i for (FD) are restricted to the coordinates $f_{i,j,k}$ such that $v_k \in [-8,8]$.

Figure (3) illustrates the very short-time behaviour of both codes. At time $t = 0$, the initial conditions are chosen so that $E = \rho = 0$, corresponding to a neutral plasma. The initial velocity field is then given by $(v, 0)$, and we observe the shear of the initial conditions. The electric field conserve the same variations through both codes, with a difference in scale.

The same simulation at time $T = 0.1$ shows a greater divergence between both methods. The electric field does not have the same extremal values, and the comparison of ρ reveals a difference of variations. The

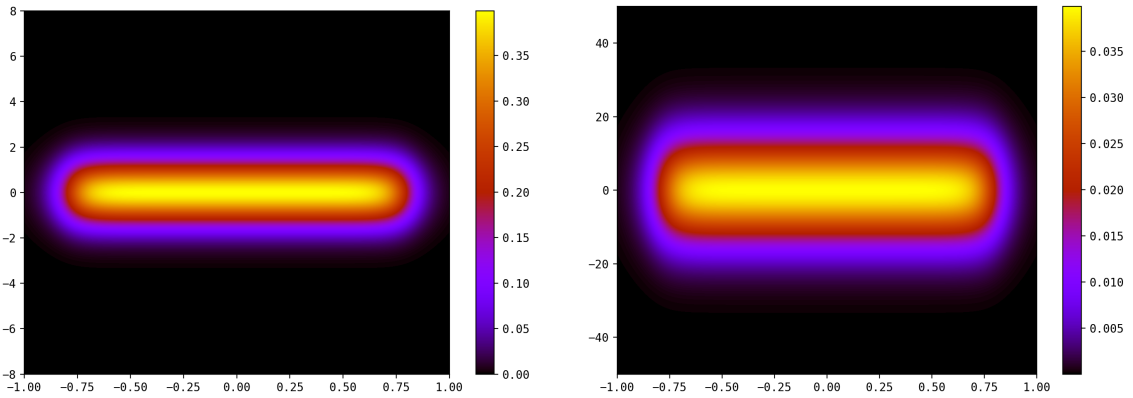

Figure 2: Initial conditions f_i^0 (left) and f_e^0 (right).

approximations of the ion density f_i seem quite similar, but the shape of the electric density f_e differs: the semi-lagrangian code produces sharper approximation and a more elongated profile.

Long time Now, we turn to the long-term simulations, with $T = 200$. Here, we free the semi-Lagrangian code from the artificial CFL condition imposed for fair comparisons. Figure (5) illustrates the behavior of both codes on long time, with parameters given by (3.5).

The finite difference code suffers from its diffusion, and the approximations of f_i and f_e are almost everywhere reduced to 0. The point $(x = 0, v = 0)$ stands out, since it is an equilibrium point: the value $f_e(t, 0, 0)$ is constant with respect to t (both in the continuous model, and in the discrete model provided $(x = 0, v = 0)$ belongs to the mesh), and

$$\partial_t f_i(t, 0, 0) = f_e(t, 0, 0), \quad \text{so that} \quad f_i(t, 0, 0) = f_i(0, 0, 0) + t f_e(0, 0, 0).$$

This explains the results of fig. (5). The value $f^n_{e,j_0,k_0} \simeq f_e(T, 0, 0)$ is stationary, but the maximum of f^n_e outside a small neighbourhood of $(x = 0, v = 0)$ is 0 at machine precision. The value $f^n_{i,j_0,k_0} \simeq f_i(T, 0, 0)$ is not taken into account in the colormap, since

$$\max_{j,k} f^n_{i,j,k} = f^n_{i,j_0,k_0} = 159.97581842617524, \quad \text{and} \quad \left| f^n_{i,j_0,k_0} - (f^0_{i,j_0,k_0} + T\nu f^0_{e,j_0,k_0}) \right| = 8.98 \times 10^{-9}.$$

At the opposite, the semi-lagrangian scheme does not produce vanishing approximations.

References

[BBC21] Mehdi Badsi, Christophe Berthon, and Anaïs Crestetto. A stable fixed point method for the numerical simulation of a kinetic collisional sheath. *Journal of Computational Physics*, 429:109990, March 2021.

[BMG+] Emily Bourne, Yann Munschy, Virginie Grandgirard, Michel Mehrenberger, and Philippe Ghendrih. Non-Uniform Splines for Semi-Lagrangian Kinetic Simulations of the Plasma Sheath. page 35.

[BMN] Mehdi Badsi, Michel Mehrenberger, and Laurent Navoret. Numerical stability of plasma sheath. page 16.

[CL20] Jean-François Coulombel and Frédéric Lagoutière. The Neumann numerical boundary condition for transport equations. *Kinetic & Related Models*, 13(1):1–32, 2020.

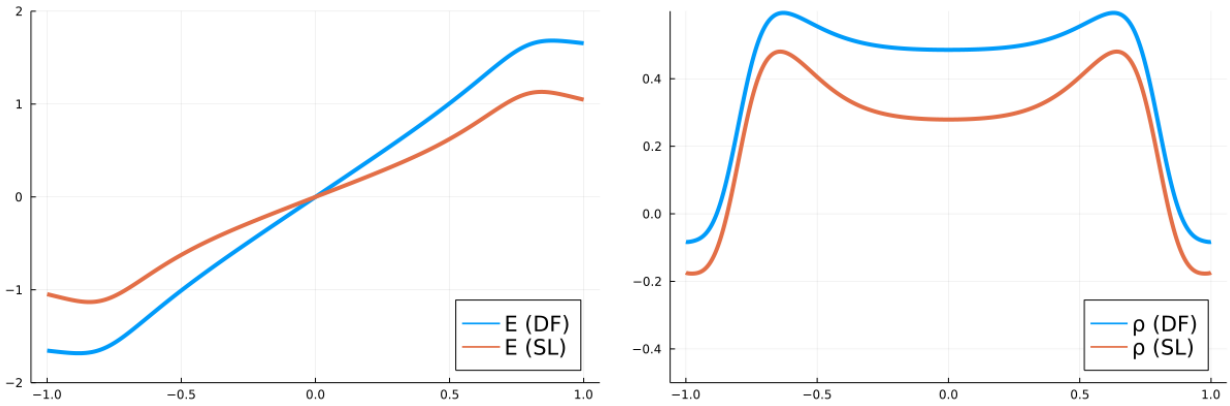

(a) Electric field (left) and density ρ (right)

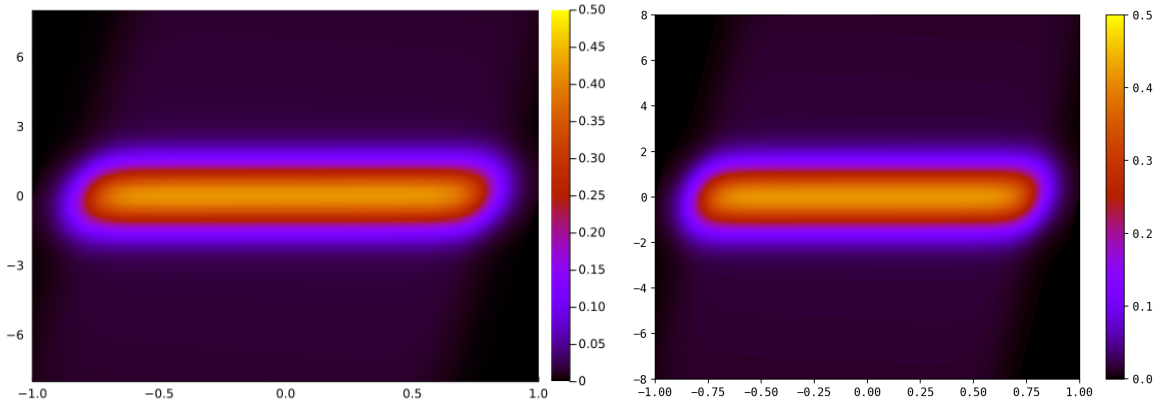

(b) Ion density

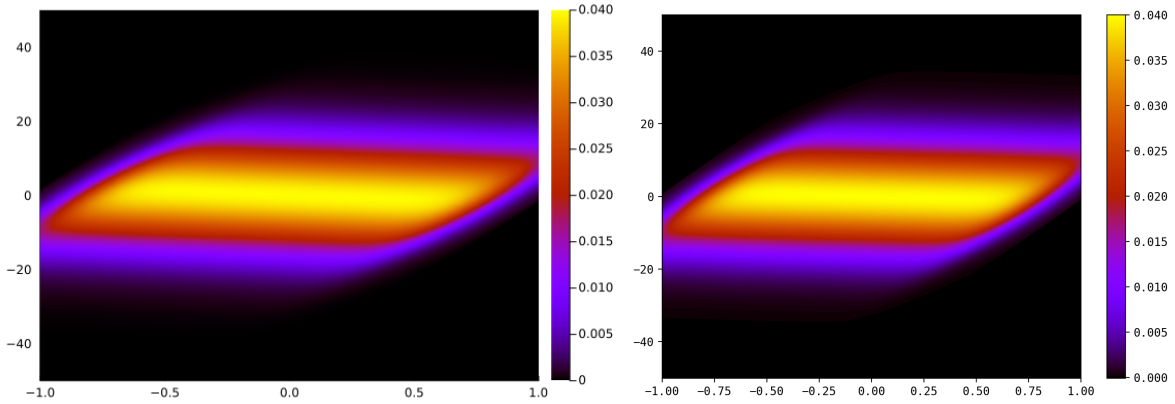

(c) Electron density

Figure 3: Comparison between finite differences (left) and semi-Lagrangian (right) at $T = 0.025$.

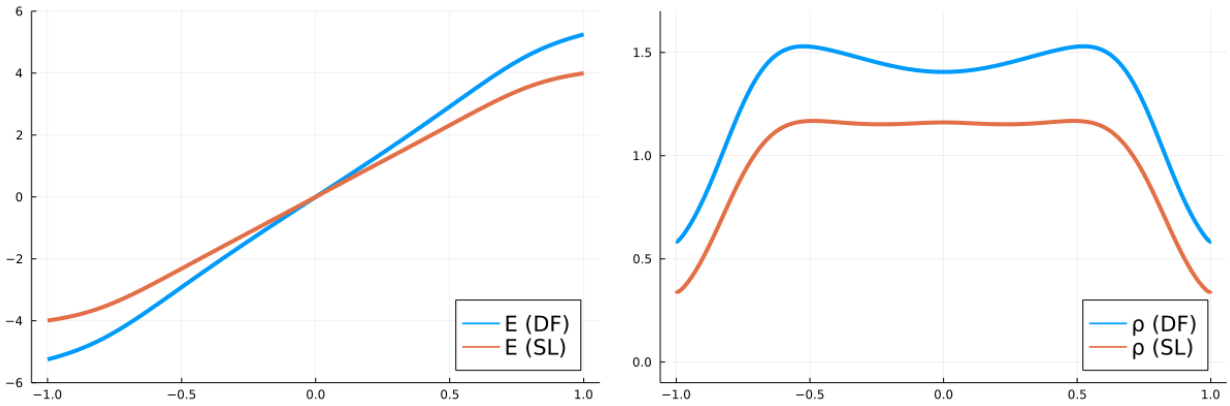

(a) Electric field (left) and density ρ (right)

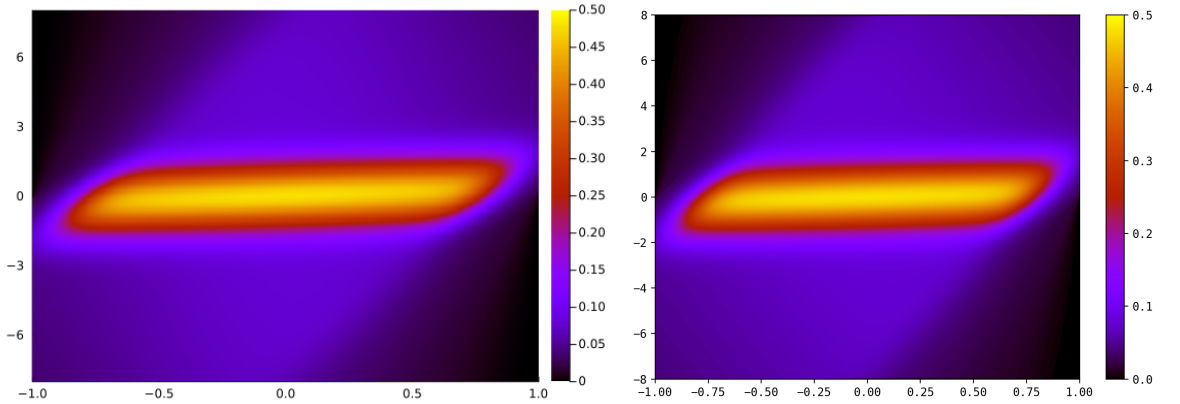

(b) Ion density

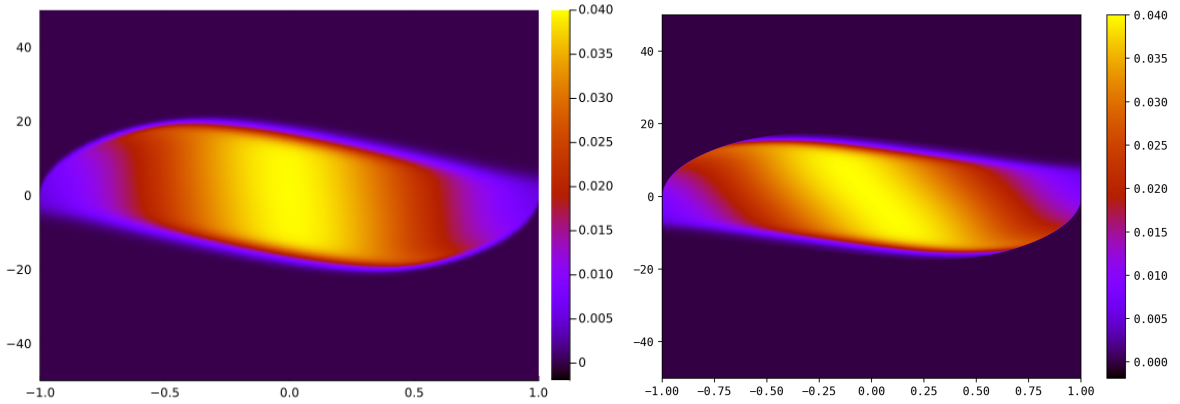

(c) Electron density

Figure 4: Comparison between finite differences (left) and semi-Lagrangian (right) at $T = 0.1$.

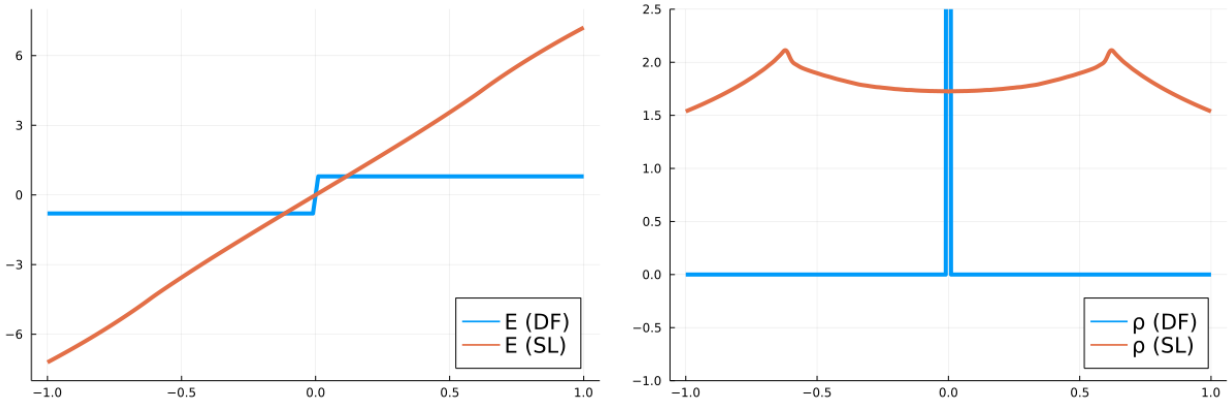

(a) Electric field (left) and density ρ (right)

The maximum of ρ for the (DF) code is equal to 39.983965094090.

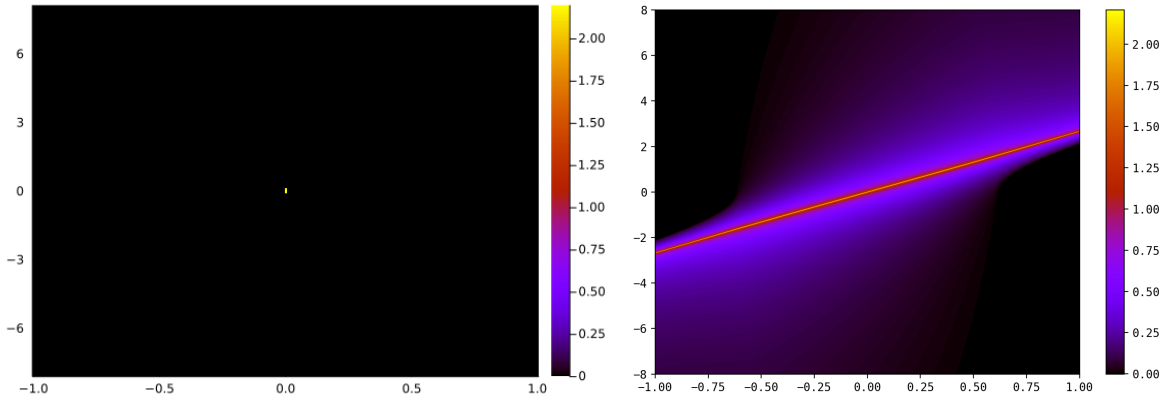

(b) Ion density

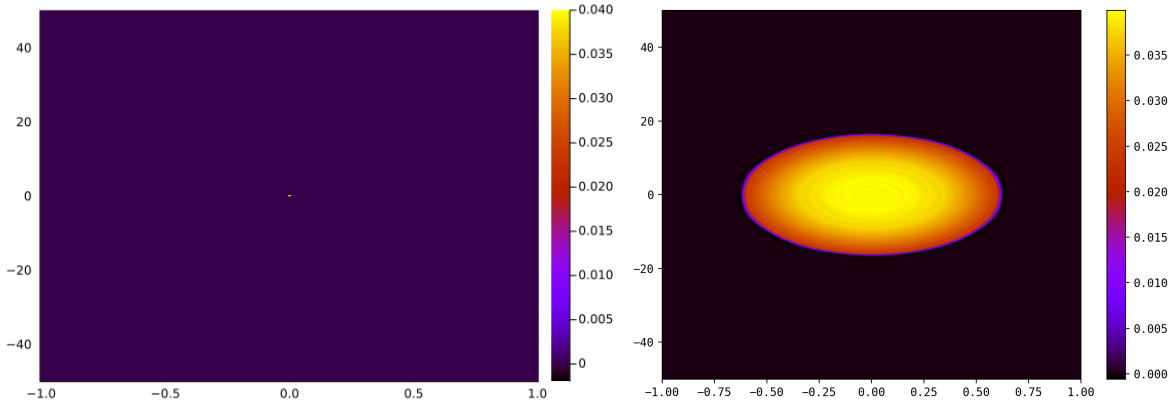

(c) Electron density

Figure 5: Comparison between finite differences (left) and semi-Lagrangian (right) at $T = 200$.

[GAB+16] V. Grandgirard, J. Abiteboul, J. Bigot, T. Cartier-Michaud, N. Crouseilles, G. Dif-Pradalier, Ch. Ehrlacher, D. Esteve, X. Garbet, Ph. Ghendrih, G. Latu, M. Mehrenberger, C. Norscini, Ch. Passeron, F. Rozar, Y. Sarazin, E. Sonnendrücker, A. Strugarek, and D. Zarzoso. A 5D gyrokinetic full- f global semi-Lagrangian code for flux-driven ion turbulence simulations. *Computer Physics Communications*, 207:35–68, October 2016.

[MK20] Evgeny A. Malkov and Alexey N. Kudryavtsev. Non-stationary Antonov self-gravitating layer: Analytics and numerics. *Monthly Notices of the Royal Astronomical Society*, 491:3952–3966, January 2020.